

**1 Contribution of hurricanes to the air-sea CO₂ flux: a
2 global view**

M. Levy¹, M. Lengaigne^{1,5}, L. Bopp², E. M. Vincent¹, G. Madec^{1,4}, C. Ethé³,
D. Kumar⁵ and V. V. S. S. Sarma⁵

¹LOCEAN-IPSL,
CNRS/IRD/UPMC/MNHN, Paris, France.

²LSCE-IPSL, CNRS/CEA/UVSQ, Saclay,
France.

³IPSL,
CNRS/IRD/UPMC/UVSQ/CEA/X/ENS/CNES/UDD/UPEC,
Guyancourt, France

⁴NOCS, Southampton, UK

⁵NIO, Goa, India.

3 **Abstract.** Previous case studies have illustrated the strong local influ-
4 ence of tropical cyclones (TCs) on CO₂ air-sea flux (F_{CO_2}), suggesting that
5 they can significantly contribute to the global F_{CO_2} . In this study, we use
6 a state-of-the art global ocean biochemical model driven by TCs wind forc-
7 ing derived from a historical TCs database, allowing to sample the F_{CO_2} re-
8 sponse under 1663 TCs. Our results evidence a very weak contribution of TCs
9 to global F_{CO_2} , one or two order of magnitude smaller than previous esti-
10 mates extrapolated from case studies. This result arises from several com-
11 peting effects involved in the F_{CO_2} response to TCs, not accounted for in pre-
12 vious studies. While previous estimates have hypothesized the ocean to be
13 systematically oversaturated in CO₂ under TCs, our results reveal that a sim-
14 ilar proportion of TCs occur over oversaturated regions (i.e. the North At-
15 lantic, Northeast Pacific and the Arabian Sea) and undersaturated regions
16 (i.e. Westernmost North Pacific, South Indian and Pacific Ocean). Conse-
17 quently, by increasing the gas exchange coefficient, TCs can generate either
18 instantaneous CO₂ flux directed from the ocean to the atmosphere (efflux)
19 or the opposite (influx), depending on the CO₂ conditions at the time of the
20 TC passage. A large portion of TCs also occurs over regions where the ocean
21 and the atmosphere are in near equilibrium, resulting in very weak instan-
22 taneous fluxes. Previous estimates did also not account for any asynchronous
23 effect of TCs on F_{CO_2} : during several weeks after the storm, oceanic pCO₂
24 is however reduced in response to vertical mixing, which systematically causes
25 an influx anomaly. This implies that, contrary to previous estimates, TCs

26 weakly affect the CO₂ efflux when they blow over supersaturated areas be-
27 cause the instantaneous storm wind effect and post-storm mixing effect op-
28 pose with each other. In contrast, TCs increase the CO₂ influx in undersat-
29 urated conditions because the two effects add up. These compensating ef-
30 fects result in a very weak contribution to global F_{CO_2} and a very modest
31 contribution to regional interannual variations (up to 10%).

1. Introduction

32 Tropical cyclones (TCs), also often called typhoons in the Northwest Pacific or hur-
33 ricanes on the eastern side of the dateline, are recurring extreme summertime weather
34 events which strongly affect the thermal and physical structure of the upper ocean along
35 their wake [e.g. *D'Asaro, 2003; Cione and Uhlhorn, 2003*]. One of the strong oceanic
36 response commonly observed in the wake of TCs is the intense cooling of the surface layer
37 that can reach up to 10°C [*Chiang et al., 2011*]. This cooling mainly ensues from the
38 wind-driven vertical entrainment of cold subsurface waters [*Price, 1981; Vincent et al.,*
39 *2011a*].

40 A few previous case studies have illustrated that TCs can cause enormous effluxes of
41 CO₂ between the ocean and atmosphere (hereafter F_{CO_2}), large enough to influence the
42 annual local efflux [*Bates et al., 1998; Perrie, 2004; Nemoto et al., 2009*]. Although TCs
43 are short-lived and travel at considerable speed (typically 4-6 m/s), they affect a significant
44 area of the tropical ocean each year, because of their large spatial extent [several ~100 km,
45 *Willoughby et al., 2006*] and frequent occurrence (~ 100 TCs each year). It is thus likely
46 that they exert a significant influence on the global air-sea flux of CO₂. However, the
47 limited availability of pCO₂ data under TCs (due to the severe weather conditions) has
48 so far restricted the global quantification of the F_{CO_2} response to TCs to qualitative
49 extrapolations [*Bates et al., 1998; Bates, 2007; Huang and Imberger, 2010*].

50 The F_{CO_2} response to a hurricane passage depends on various factors. F_{CO_2} is a function
51 of piston velocity and of the difference in the partial pressure of CO₂ (pCO₂) between the
52 atmosphere and sea surface. Oceanic pCO₂ depends on total dissolved inorganic carbon

53 (DIC), total alkalinity (TA), temperature (T) and salinity (S) [*Takahashi et al.*, 1993].
54 TCs increase the magnitude of the F_{CO_2} because the piston velocity strongly increases
55 at high wind speed [*Liss and Merlivat*, 1986; *Wanninkhof*, 1992; *D’Asaro and McNeil*,
56 2007; *McNeil and D’Asaro*, 2007]. TCs also impact F_{CO_2} because their intense surface
57 winds increase vertical entrainment of subsurface waters (hereafter referred to as mixing)
58 and thereby change the surface properties of T, S, DIC and TA and thus surface oceanic
59 pCO₂. In addition, the net F_{CO_2} response to TCs is complicated by the fact that the
60 TC-induced mixing (affecting the pCO₂) and TC-winds (affecting the piston velocity)
61 are not synchronous [*Nemoto et al.*, 2009]: cooling, the manifestation of vertical mixing,
62 is observed to be maximum between one and three days after the TC-passage [*Vincent*
63 *et al.*, 2011b] and its intensity depends on the local vertical structure of the upper ocean
64 [*Vincent et al.*, 2011a].

65 These considerations highlight the difficulty in generalizing the F_{CO_2} response to TCs
66 from individual cases and illustrate why the few global TC-induced F_{CO_2} estimates [*Bates*
67 *et al.*, 1998; *Bates*, 2007; *Huang and Imberger*, 2010] are so disparate: from ~ 0.5 PgC to
68 ~ 0.05 PgC per year. This paper proposes an original methodology and a model framework
69 for accurately quantifying the TC-induced F_{CO_2} and the various processes into play. We
70 use a global Ocean General Circulation Model [NEMO, *Madec*, 2008] coupled with a bio-
71 geochemical model [PISCES, *Aumont and Bopp*, 2006] with a modified version of CORE
72 forcing [*Large and Yeager*, 2009] that includes an analytic formulation of 2-dimensional
73 TC winds along observed TC tracks [*Vincent et al.*, 2011a]. We compare two model sim-
74 ulations, with and without TCs, and provide quantitative diagnostics averaged along the

75 tracks of TCs. This enables us to provide a global picture of the effects of hurricanes on
76 air-sea CO₂ transfers.

2. Model and methods

2.1. Coupled hydrodynamic and carbon model

77 The hydrodynamical model used here is the global configuration (ORCA2) of Nucleus
78 for European Modelling of the Ocean [NEMO, v3.2, *Madec*, 2008]. The quasi-isotropic
79 grid has a nominal resolution of 2° with increased 0.5° latitudinal resolution at the equa-
80 tor. In the vertical, 31 levels are used, with 10 levels in the upper 100 m. The mixed layer
81 dynamics is parameterized using an improved Turbulent Kinetic Energy (TKE) closure
82 scheme with a Langmuir cell, a surface wave breaking parameterization and an energet-
83 ically consistent time and space discretization [*Madec*, 2008]. Additional subgrid-scale
84 mixing parameterizations include a Laplacian viscosity, an iso-neutral Laplacian diffusiv-
85 ity and the use of a GM-scheme to mimic the effect of subgrid-scale eddy processes [*Gent*
86 *and McWilliams*, 1990]. Complete description of ORCA2 can be found in *Cravatte et al.*
87 [2007].

88 The Pelagic Interaction Scheme for Carbon and Ecosystem Studies (PISCES, Aumont
89 and Bopp, 2006) is coupled to ORCA2. PISCES includes a simple representation of the
90 marine ecosystem and describes the cycles of carbon and of the main marine nutrients
91 (N, P, Fe and Si). The model has 24 compartments. Four living pools are represented:
92 two phytoplankton size classes/ groups (nanophytoplankton and diatoms) and two zoo-
93 plankton size classes (microzooplankton and mesozooplankton). Fixed Redfield ratios are
94 employed for N and P, while the ratios of both Si, and Fe, to C vary dynamically as a
95 function of the phytoplankton functional group and environmental variables. The carbon-

96 ate chemistry follows the Ocean Carbon-Cycle Model Intercomparison Project (OCEMIP)
 97 protocols (www.ipsl.jussieu.fr/OCMIP). The air-sea CO₂ exchange is calculated with the
 98 bulk exchange formula:

$$F_{CO_2} = k s DpCO_2 \quad (1)$$

99 where F_{CO_2} is the air-sea CO₂ flux with positive values indicating CO₂ goes within the
 100 ocean, k is the gas transfer velocity, s is the CO₂ solubility and $DpCO_2 = pCO_2^{atm} - pCO_2^{sea}$
 101 is the difference of pCO₂ between the ocean and atmosphere. In the following, we will use
 102 the notation pCO₂ for pCO₂^{sea}. There is still large uncertainty in k , particularly under
 103 hurricane winds [*McNeil and D'Asaro, 2007; D'Asaro and McNeil, 2007*]. Following the
 104 discussion by *McNeil and D'Asaro [2007]*, we used the relationship of *Wanninkhof [1992]*
 105 to calculate k , which provides a lower limit for k under extreme winds compared to other
 106 recent formulations [*Perrie, 2004*].

2.2. Model set up and experimental design

107 The surface boundary conditions used for the present ORCA2-PISCES simulations are
 108 based on the version 2 of the atmospheric data sets and formulations developed by Large
 109 and Yeager (2009) for global ocean-ice models and are referred to as Coordinated Ocean-
 110 ice Reference Experiments (CORE) forcing [*Griffies et al., 2009*]. The forcing data sets
 111 are based on a combination of NCEP/NCAR reanalysis products for the years 1958-2007
 112 with various satellite data sets, and involve adjustments that correct global imbalances
 113 (e.g., produce near zero global mean heat and freshwater fluxes when used in combination
 114 with observed SSTs). Turbulent fluxes are computed from the CORE bulk formulae

115 as a function of the prescribed atmospheric state and the simulated ocean surface state
116 (SST and surface currents). A bound to 33 m s^{-1} has been introduced to the CORE
117 dimensionless surface drag coefficient (C_D) to account for its observed saturation at strong
118 winds following *Donelan* [2004]. Data are prescribed at six-hourly (wind speed, humidity
119 and atmospheric temperature), daily (short- and long-wave radiation) and monthly (rain
120 and snow) resolution, with inter-annual variability over the time range 1958 to 2007
121 except for runoff which are kept climatological. To avoid an artificial model drift due
122 to a freshwater imbalance, the sea surface salinity is damped towards monthly-mean
123 climatological values with a piston velocity of 50 m per 300 days [*Griffies et al.*, 2009].

124 Boundary conditions for the biogeochemical model include atmospheric dust (Fe) de-
125 position, rivers (Fe, N, P, Si and C) and sediment (Fe) mobilization. These sources are
126 described in *Aumont and Bopp* [2006] and kept constant for the duration of the simulation.

127 Our simulations start in 1978. For the initial state, we used physical and biogeochemi-
128 cal tracers initialized from previous ORCA2-PISCES experiments: the spun-up physical
129 state was obtained by running a 120-year simulation, starting from Levitus and forced by
130 repeating the 50-year CORE forcing; the biogeochemical state was obtained by running a
131 transient 1870-1977 simulation with increasing pCO_2^{atm} levels following historical records.

132 From 1978 onwards, we performed two simulations: one with the full strength of TCs
133 (Cyclone or C run) and one without TCs (No cyclone or N run). For these simulations,
134 the 10-m wind forcing from CORE has been modified following *Vincent et al.* [2011b]:
135 In the N run, the effect of the weaker than observed TC-like vortices seen in the original
136 CORE forcing has been filtered out by applying a 11-day running mean to the wind
137 components within 600km of each cyclone (Fig. 1). In the C run, analytical TCs have

138 been superimposed to the filtered CORE winds. To do so, TC winds are parameterized
139 using the idealized *Willoughby and Rahn* [2004] TC wind spatial pattern, which is based
140 on a statistical fit to the observed TC winds [*Willoughby et al.*, 2006]. This idealized wind
141 pattern is interpolated in time at each model time step using the position and maximum
142 wind speed of each cyclone in the IBTrACs database (www.ncdc.noaa.gov/oa/ibtracks).
143 This analytical formulation enables to correct for the underestimation of the strength of
144 TC-winds in CORE. Fig. 1 provides an illustration of the different wind forcings (CORE,
145 N and C) under a TC in the south-west Indian Ocean.

146 Daily model outputs were saved from 1993 onward. Our analysis are thus based on the
147 1993-2007 period, and sample the ocean’s response to 1663 TCs.

2.3. Diagnostics of oceanic anomalies generated by TCs along their tracks

148 The anomalies of a given oceanic variable V (where V is for instance the temperature or
149 $p\text{CO}_2$) ensuing from the passage of TCs, noted ΔV , are computed under each TC track.
150 To compute ΔV , the seasonal cycle of V is first removed from V . TC track locations,
151 available at 6h intervals, are used to retrieve V at the surface of the ocean. To character-
152 ize the amplitude of the ocean response around each TC-track position, we compute \mathcal{V} ,
153 the average of seasonally-detrended V over a fixed radius of 200km (about 3-4 radius of
154 maximum wind) around the track position. We do this averaging because the impact of
155 TCs on sea-surface properties is not restricted to a narrow path along the storm’s center
156 but rather can occur in a swath hundreds of kilometers wide, as reported for instance by
157 *Bond et al.* [2011]. The reference unperturbed pre-storm conditions (\mathcal{V}_{before}) is defined
158 as the average of \mathcal{V} over 10 to 3 days prior to TC passage. The evolution of the ocean
159 response anomaly at time t to a TC is then defined as $\Delta V(t) = \mathcal{V}(t) - \mathcal{V}_{before}$. The post-

160 storm anomalies $\Delta V(t)$ are generally maximum within 1 to 4 days after the TC passage
 161 (section 3.1). We define \mathcal{V}_{after} as the mean value of \mathcal{V} over days 1 to 4 after TC passage,
 162 and the wake anomaly as $\overline{\Delta V} = \mathcal{V}_{after} - \mathcal{V}_{before}$ (Fig. 2).

163 This methodology is applied to the model runs and to satellite observations of SST. In
 164 the N-run, where TCs have been smoothed out, ΔV_N is close to zero but is not strictly
 165 equal to zero because of the presence of variability not due to TCs. This background
 166 variability is present in both the C and N runs. To remove it from our estimates of ΔV ,
 167 for model variables we define ΔV as $\Delta V = \Delta V_C - \Delta V_N$, where subscripts N and C refer
 168 to the model solutions of the N and C runs, respectively. Removing ΔV_N does not change
 169 our main results and reduces the dispersion (not shown).

2.4. Air-sea flux anomaly diagnostics

170 Anomalies in F_{CO_2} in response to TCs (ΔF_{CO_2}) can result either from changes in the
 171 wind (and thus in gas transfer velocity Δk) or from changes in mixing (and thus in
 172 $\Delta(s DpCO_2)$):

$$\Delta F_{CO_2} = \underbrace{\Delta k \times s DpCO_2}_{\text{wind effect}} + \underbrace{k \times \Delta(s DpCO_2)}_{\text{mixing effect}} \quad (2)$$

173 Using the results from the C and N runs, the wind and mixing effects are approximated
 174 as :

$$\Delta k \times s DpCO_2 \simeq (k_C - k_N) \times s_N (DpCO_2)_N \quad (3)$$

and

$$k \times \Delta(s DpCO_2) \simeq k_N \times (s_C (DpCO_2)_C - s_N (DpCO_2)_N) \quad (4)$$

175 where subscripts N and C refer to the model solutions of the N and C runs, respectively.
176 Note that the second order terms have been omitted in this approximation; a posteriori,
177 our results show that they are smaller than the first order terms.

3. Model evaluation

3.1. Evaluation of TC-induced cooling

178 The C run captures very accurately the timing of the average observed cooling (Fig.
179 2a). In both model and observation, the temperature decrease starts a few days before the
180 wind reaches its peak intensity at a given location (Day 0) and reaches its maximum am-
181 plitude 2-3 days after the TC passage. The cold anomaly persists for several weeks after
182 the TC passage and is largely restored after 40 days. We note however that SST remains
183 on average 0.2° colder than pre-storm conditions, in agreement with other observational
184 analysis [*Price et al.*, 2008; *Lloyd and Vecchi*, 2011; *Vincent et al.*, 2011a]. Based on this
185 composite picture, the average value of the e-folding time (time for the cold anomaly to be
186 reduced by a factor e) is 15 days. Moreover, there is a 0.68 correlation between modeled
187 and observed TC-induced cooling magnitudes ($\overline{\Delta T}$) in the wake of TCs at individual lo-
188 cations (Fig 2b), indicating that our simulation realistically samples the ocean response to
189 the wide spectrum of TC characteristics. Because the analytic cyclone wind field formula-
190 tion is fitted to an average of observed cyclone wind radial profiles [*Willoughby and Rahn*,
191 2004], we however do not expect each simulated cold wake to match the corresponding
192 observed one, as illustrated by the spread on Fig. 2b. The model also successfully repro-
193 duces the observed spatial distribution of the TC-induced cooling (Fig. 3): the average
194 cooling within TC-active regions is about 1°C in all basins, with maximum amplitude of
195 about 2°C in the north-west Pacific region where amongst the most intense TCs occur.

196 The main model deficiency lies in the North-East Pacific basin where modeled coolings
197 are overestimated by almost 1°C. This bias can be tracked back to a shallower than ob-
198 served thermocline in this region. The use of a coarse horizontal resolution (2°) in our
199 simulation do not hinder the realism of the ocean response to TCs: similar comparisons
200 to observations have indeed been obtained with a simulation of higher (0.5°) resolution
201 using similar boundary conditions and forcing strategy [Fig. 2 in *Vincent et al.*, 2011a].

3.2. Evaluation of the DpCO₂

202 Simulated DpCO₂ has been evaluated against observations-based climatologies in *Au-*
203 *mont and Bopp* [2006] both in terms of annual-mean, seasonal amplitude and phasing.
204 Here, we focus on the mean DpCO₂ during the TC-season, i.e. from November to April
205 in the southern hemisphere and from May to October in the northern hemisphere (Fig.
206 4). The TC-season DpCO₂ displays regions both with positive and negative values qual-
207 itatively well reproduced by the model. Regions with negative DpCO₂ (oceanic sources
208 of CO₂ to the atmosphere) are in the tropical eastern Pacific, the tropical Atlantic, the
209 Arabian sea. Regions with positive DpCO₂ (oceanic sinks for atmospheric CO₂) are found
210 off the west coast of Australia, in the Southwest Pacific and in the mid-latitudes of all
211 oceanic basins.

4. Results

4.1. Case of TC Felix at station BATS

212 The observations of *Bates et al.* [1998] at station BATS (31°10'N, 64°10'W) in the
213 Western North Atlantic before and after the passage of TC Felix provide a unique oppor-
214 tunity to evaluate the response in pCO₂ predicted by our model. Around BATS, typical

215 summertime conditions are characterized by weak winds and seawater pCO₂ larger than
216 atmospheric pCO₂^{atm} levels, causing a small flux from ocean to atmosphere. Felix passed
217 over the station on 14-15 August 1995. It was quite large (350 km in diameter) and had
218 sustained winds of 40-45 $m s^{-1}$. For several weeks before the storm, the SST was close to
219 28°C and pCO₂ ranged from 400-420 μatm . A sharp decrease of SST and pCO₂ occurred
220 following the TC passage, with similar amplitudes in both model and observations (resp.
221 -3C and -45 μatm). The SST and pCO₂ rebounded after passage of Felix, but did not
222 return to pre-storm values (data from Bates et al., 1998, reproduced in Fig. 5a,b). The
223 oceanic response to Felix is hence successfully captured by our simulation although the
224 absolute pCO₂ values display a $\sim 10\mu atm$ systematic shift in our experiment (Fig. 5a,b),
225 which is rather understandable given the coarse model resolution used here.

226 The TC passage results in significant changes of the modeled F_{CO_2} (Fig. 5c). In the
227 C-run, the F_{CO_2} peaks very abruptly during the 2-days corresponding to the TC passage
228 (August 14-15) reaching 58 mmole/m²/day, then nearly vanishes (from August 16-29)
229 until three other storms hit the area (in September). In the N-run, the F_{CO_2} do not
230 experience any large variations during the passage of the main TC and of the subsequent
231 storms compared to the C-run, but is larger during the more quiet periods (Fig 5c,d).

232 To interpret the differences of F_{CO_2} between the 2 runs, the wind and mixing effects
233 have been separated according to equations 2, 3 and 4 applied at the fixed location of
234 BATS (Fig. 5d). This diagnostics clearly reveals that the wind effect is the driver of the
235 strong increase of F_{CO_2} during the 2 days of the TC-passage and of the three subsequent
236 storms (green curve in Fig. 5d). On the other hand, the mixing effect (blue curve in
237 Fig. 5c) acts to increase the pCO₂ and thus to reduce the ΔpCO_2 , which reduces the

238 F_{CO_2} ; moreover, the mixing effect is lagged and last longer compared to the wind effect,
239 reducing F_{CO_2} for more than 2 weeks reaching a maximum 2-3 days after the passage of
240 Felix.

241 The F_{CO_2} caused by Felix has been previously estimated by *Bates et al.* [1998], by
242 assuming that the oceanic pCO₂ was constant in the lead up of the storm, then decreased
243 linearly to the end of the hurricane. This led to a total flux of 40 mmoleC m⁻² during
244 the two-days passage of the storm; this estimate did not account for the flux reduction
245 during post-hurricane conditions. With our model, we predict a $\tilde{\Delta}F_{CO_2}$ of 62 mmoleC m⁻²
246 during the storm. This larger number compared with to *Bates et al.* (1998) is due to
247 the slower decrease of the oceanic pCO₂ in the model compared to the linear decrease
248 hypothesized by *Bates et al.* (1998). *Koch et al.* (2009) also estimated the $\tilde{\Delta}F_{CO_2}$ caused
249 by Felix during the two-days of the storm with a regional model, forced with daily NCEP
250 winds. They found a lower value than *Bates et al.* (1998) of 32 mmoleC m⁻², which they
251 attribute to the underestimation of their model wind forcing. In a second step, to account
252 for the post-storm effect, we integrate the impact of TC Felix over two weeks. In this case,
253 the increase of the $\tilde{\Delta}F_{CO_2}$ during the TC passage is counter-balanced by an the increased
254 during post-TC conditions by approximately half, which leads to the final estimate of 30
255 mmoleC m⁻². This post-storm effect was not accounted for in the estimates of *Bates et al.*
256 [1998] and *Koch et al.* [2009].

257 A situation similar to that observed at BATS by *Bates et al.* [1998] was reported by
258 *Nemoto et al.* [2009] in the coastal East China Sea, from continuous temperature and pCO₂
259 measurements at a moored buoy. Because their buoy was located in a coastal area, we
260 cannot directly compare their observations with our 2° model results. However, *Nemoto*

261 *et al.* [2009] examined how the variations in wind and in pCO₂ affected the F_{CO_2} . They
262 found, in agreement with our analysis at BATS, that the F_{CO_2} efflux is increased during
263 the passage of the storm, because of the increase in wind speed, and is decreased after the
264 storm has passed, because of the decrease of pCO₂. Nevertheless, their estimate of the
265 impact of TCs on the F_{CO_2} , approximately 30 mmoleC m⁻² per typhoon, only accounts
266 for the wind effect.

4.2. Sign of DpCO₂ under TCs

267 The efflux observed at BATS during TC Felix results from the negative DpCO₂ at the
268 time t_0 of the TC passage. Previous studies that attempted to estimate the global impact
269 of TC on F_{CO_2} have generalized this observation, hypothesizing that DpCO₂ at t_0 was
270 negative for all TCs. Our numerical experiment allows to check this hypothesis (Fig. 6):
271 we found almost as many occurrences of negative and positive DpCO₂ at t_0 (25773 versus
272 21178 cases). The immediate consequence is that TCs do not systematically cause CO₂
273 effluxes at t_0 (as in BATS) but also be responsible for influxes, in similar proportion (Fig.
274 6b). Moreover, $|DpCO_2|$ at t_0 is larger than 10 μatm in $\sim 50\%$ of the cases, and cause the
275 largest F_{CO_2} anomalies (tails of the distribution in Fig. 6b). In the other $\sim 50\%$ cases,
276 the impact of TC on the F_{CO_2} is small because DpCO₂ is close to zero.

277 The spatial distribution of the positive and negative DpCO₂ cases under TCs in the C-
278 run is displayed in Fig. 7a,b. Areas with negative DpCO₂ during the cyclonic seasons are
279 found mostly in the Western North Atlantic, Western and Eastern North Pacific, Arabian
280 Sea and South West Indian Ocean, while areas of positive DpCO₂ are mostly in the
281 Westernmost North Pacific, central south Indian Ocean, Bay of Bengal and South western
282 Pacific, in broad agreement with the pCO₂ distribution during the cyclonic season (Fig.

283 4). The same diagnostic applied to the climatology of *Takahashi et al.* [2009] interpolated
284 in time reveals similar regional patterns (Fig. 7c,d). The differences are due both to
285 model imperfections and to the absence of interannual variations in the climatology.

4.3. TCs induced DpCO₂ and F_{CO_2} anomalies

286 Since the F_{CO_2} response differ depending on the sign of the DpCO₂ background condi-
287 tions at the time of TCs passage, two different cases are considered in the following: the
288 case where DpCO₂ is negative at t_0 , causing an efflux to the atmosphere (case of BATS),
289 and the opposite case, where DpCO₂ is positive at t_0 , causing an influx to the ocean.
290 Figure 8 shows the composite evolution of wind speed, SST, DpCO₂ and F_{CO_2} anomalies
291 associated with the passage of all TCs falling in each category, and computed following
292 section 2.3.

293 In the two cases, the composite time-evolution of the wind, SST and DpCO₂ TC-induced
294 anomalies are consistent with the results obtained in the case of TC Felix at BATS: TCs
295 induce a cooling of the SST (Fig. 8b), which reaches its maximum amplitude two to three
296 days after the maximum wind speed intensity and slowly returns to its pre-storm value
297 during the month that follows the passage of the TC. In our simulation, the maximum
298 coolings reach 4°C, and the mean cooling when averaged over all TCs is less than 1°C. In
299 agreement with *Vincent et al.* [2011b], this cooling mainly results from the entrainment
300 of cold sub-surface waters driven by the storm, especially for the strongest wind forcing.
301 The mean cooling is larger in the negative DpCO₂ case, because different oceanic regions
302 are concerned in the two cases. Vertical mixing not only decreases SST but also, in
303 agreement with the theoretical pCO₂ change with temperature [*Sarmiento and Gruber,*
304 2006], decreases pCO₂ and thus increases DpCO₂ (Fig. 8c). Moreover, as for SST, the

305 maximum magnitude of the pCO₂ drawdown is reached 2 to 3 days after the passage of
306 the storm (Fig. 8c), and the change is larger in the negative DpCO₂ case.

307 Because the pre-storm air-sea fluxes have different signs in the two cases, the direct
308 impact of TC winds on the air-sea CO₂ fluxes are opposite. At t_0 , TC winds acts to
309 increase the amplitude of the flux in either direction, thus enhancing effluxes in the case
310 of negative DpCO₂, and enhancing influxes in the case of positive DpCO₂ (Fig. 8). After
311 the storm, the decrease of pCO₂ causes $|DpCO_2|$ to decrease in the negative DpCO₂
312 (undersaturated) case (and eventually change sign), and to increase in the positive DpCO₂
313 (oversaturated) case (Fig. 9); consequently, the amplitude of the flux is reduced in the
314 oversaturated case (and eventually reverses), and is increased in the undersaturated case,
315 in comparison with pre-storm conditions (Fig. 8 and 9).

4.4. Respective influence of TCs wind and induced mixing on F_{CO_2}

316 To assess and quantify the impact of TCs on F_{CO_2} , the wind and mixing effects have
317 been separated according to equations 2, 3 and 4 for each TC, and averaged out for all
318 oversaturated (resp. undersaturated) cases (Fig. 10). In both cases, the wind effect
319 explains most of the increase of the flux in either direction during the TC-passage, while
320 the mixing effect explains the modifications of the flux after the storm, in opposite sign
321 in the case of oversaturation, and in same sign in the case of undersaturation.

322 In the oversaturated case, when integrated over 30 days, the time integral of the TC-
323 induced flux anomaly is 1.1 mmole/m² and is positive. This means that, on average over
324 all TCs, the negative wind-driven flux anomaly during the storm is more than offset by the
325 post-storm, positive, mixing-driven flux anomaly. In the undersaturated case, the time

326 integral of the TC-induced flux anomaly is 10.1 mmole/m²; in this case, the wind-driven
327 and mixing-driven anomalies are both positive and add up.

4.5. Regional and global impact of TC on F_{CO_2}

328 In Figure 11, the storm and post-storm impacts of TCs on F_{CO_2} are evaluated regionally.
329 This is done by integrating ΔF_{CO_2} over two time periods.

330 During the storm peak intensity ($t_0-1.5d$ to $t_0+1.5d$, Fig. 11b), the averaged TC-driven
331 flux anomaly is negative in the North West Atlantic, North West Pacific, North East
332 Pacific, Arabian Sea and South West Indian, and is positive in the Westernmost North
333 Pacific, central south Indian Ocean, Bay of Bengal and South western Pacific. These
334 patterns are due to the first (resp. second) regions being predominantly supersaturated
335 (resp. undersaturated) during the cyclonic season (Fig. 4). After the storm ($t_0+1.5d$ to
336 t_0+30d , Fig. 11c), the flux anomaly is systematically positive (except for a small region
337 in the north eastern Pacific, where pCO₂ is enhanced by vertical mixing) and its pattern
338 is that of the TC density. When considering the whole period ($t_0-1.5d$ to t_0+30d , Fig.
339 11a), the storm and post-storm effects often balance when they are of opposite signs.

340 In consequence, in the North West Atlantic and Arabian Sea, which are mostly supersat-
341 urated during the cyclonic season, the net effect of TC on F_{CO_2} during the cyclonic season
342 is very weak because the storm and post-storm effects almost compensate. The situation
343 is different in the North West Pacific, where the strongest SST anomalies occur (Fig.
344 3); because of these strong SST anomalies, the post-storm effect prevails over the storm
345 effect, with the consequence of a net TC-induced CO₂ influx anomaly. In regions which
346 are predominantly undersaturated during the cyclonic season, the storm and post-storm
347 effects reinforce each other. Consequently, the mean effect of TC in the Westernmost

348 North Pacific, central south Indian Ocean, Bay of Bengal and South western Pacific is to
349 increase the uptake of CO₂ by the ocean during the cyclonic season.

350 Tables 1 and 2 provide more quantitative numbers of the impact of TCs on F_{CO_2} over
351 the large regions delimited in Fig. 11. Except in the North West Pacific and in the Bay of
352 Bengal, the flux due to TC is generally less than $\pm 3\%$ of the total flux. In the North West
353 Pacific and Bay of Bengal the percentage is larger (+33.4 % and -13.6 %, respectively), but
354 they concern regions which weakly (15.5 and -0.6 TgC, respectively) contribute to the total
355 F_{CO_2} during the cyclonic season (-305 TgC). Note also that in most regions, the flux due to
356 TCs is not systematically in the same direction (Table 2); for instance, the North Atlantic
357 is submitted to an average of 80 TC-days over supersaturated conditions, contributing
358 to a TC efflux of -1.6 TgC, but also to 16 TC-days over undersaturated regions, which
359 cause an influx of +1 TgC. Under undersaturated conditions, the TC induced flux is
360 always positive, while it can be either positive or negative under supersaturated conditions
361 (depending on the relative strength of the storm and post-storm effects) (Table 2). The
362 North West Pacific and Bay of Bengal are predominantly undersaturated, which explains
363 the larger % of the TC-flux to the total flux.

5. Discussion

5.1. Comparison with previous estimates

364 The global impact of TCs on air-sea CO₂ fluxes estimated in this study ($0.007 Pg C y^{-1}$,
365 i.e. 2% of the mean, subtropical flux during the cyclonic season, Table 1) is one order of
366 magnitude less than the lowest previous estimates [Perrie, 2004; Bates, 2007; Koch *et al.*,
367 2009; Huang and Imberger, 2010] and is in opposite direction (influx anomaly). This is
368 because previous estimates did not account for two important aspects: first, in supersat-

369 urated regions, they did not account for the post-storm mixing-effect, which balances the
370 storm wind-effect; second, they did not consider the impact of TCs over undersaturated
371 regions.

372 Previous estimates of air-sea CO₂ fluxes under TCs mainly focused on hurricanes in
373 the North West Atlantic [*Bates et al.*, 1998; *Perrie*, 2004; *Bates*, 2007; *Koch et al.*, 2009;
374 *Huang and Imberger*, 2010], with the exception of one study in the East China Sea [*Nemoto*
375 *et al.*, 2009]. These studies took place in undersaturated regions. In most of them, it was
376 attempted to extrapolate the results from a few TCs (one to three TCs, typically) to the
377 global ocean, by using TCs database and making assumptions about storm area, wind
378 speed and oceanic pCO₂ values. Moreover, it was generally assumed that the oceanic
379 conditions at the time and location of TC passage did not significantly deviate from the
380 case study that was examined. The different assumptions and methods used led to a wide
381 range of estimates. The first global estimate by *Bates et al.* [1998] was a TC-induced
382 efflux of up to 0.51 Pg C. Later, *Bates* [2007] estimated a smaller efflux of 0.04-0.08 Pg C,
383 but no details on the method were provided. The method of *Huang and Imberger* [2010],
384 with different extrapolation assumptions, lead to an efflux of 0.047-0.141 Pg C. *Nemoto*
385 *et al.* [2009] restricted their extrapolation to the western subtropical North Pacific, and
386 found a contribution of TCs equal to 76% of the summer efflux, a value even larger than
387 the 20-54% estimate of *Bates et al.* [1998]. Our estimate in for North West Atlantic is
388 close to zero (1%, Table 1), because the wind and mixing effect are in balance. In the
389 North West Pacific, we found a larger impact (-37%, Table 1) but with opposite sign,
390 because the mixing effect is larger than the wind effect. In that respect, our results are
391 thus significantly different from the previous estimates.

392 Moreover, it was hypothesized that the year-to year differences in TC frequency and
393 intensity might be an important mechanism for controlling interannual variability in F_{CO_2}
394 [*Bates et al.*, 1998; *Bates*, 2007], although this hypothesis was not supported by the
395 model result of *Koch et al.* [2009] in the subtropical North Atlantic. To examine this
396 question over different ocean sub-basins, we compared the standard deviation of the year-
397 to-year regional F_{CO_2} budget to the the standard deviation of the year-to-year regional
398 TC-induced F_{CO_2} flux (Table 1). Our result extend the conclusion of *Koch et al.* [2009]:
399 over the different sub-basins, TC explain between 0 and 10% of the interannual flux
400 changes, with a global mean of ~ 5 %.

5.2. The post-storm, mixing effect

401 One of the important process highlighted in this study is the impact of TC-induced
402 vertical mixing with thermocline waters, which occurs essentially after the storm, cools
403 the SST and reduces the pCO₂. The importance of this processes is revealed by the
404 persistence of the cold SST anomaly after the passage of the storm that can last from a
405 few days to over a month. This persistence is accurately reproduced by our model when
406 compared with satellite AMSR observations. The link between the cooling and the change
407 in pCO₂ is however not straightforward. Figure 12 shows the distribution of the change in
408 pCO₂ after the passage of TC, against the change in SST (computed following section 2.3
409 as $\overline{\Delta pCO_2}$ versus $\overline{\Delta T}$). It confirms that in most cases, pCO₂ decreases after the passage
410 of TCs; the average decrease ($-7.6 \mu atm$ per °C) is however smaller than the theoretical
411 decrease due to the temperature effect alone ($-13 \mu atm$ per °C, *Sarmiento and Gruber*
412 [2006]). This feature can be explained by the entrainment of higher DIC water from the
413 thermocline into the surface mixed-layer which increases the pCO₂ and partly offsets the

414 temperature effect ; TC can also alleviate nutrient limitation and promote phytoplankton
415 blooms [*Babin et al.*, 2004; *Walker et al.*, 2005; *Son et al.*, 2006; *Patra et al.*, 2007; *Liu*
416 *et al.*, 2009; *Hanshaw et al.*, 2008; *Gierach and Subrahmanyam*, 2008], thus decreasing the
417 pCO₂. How mixing of these different elements impact pCO₂ depends on their respective
418 vertical gradients and is spatially and temporally variable [*Mahadevan et al.*, 2011]. Our
419 model results are in that respect consistent with the analysis of *Mahadevan et al.* [2011],
420 based on climatological distributions of T, S, DIC, nutrients and TA, which suggest that
421 the temperature impact on pCO₂ prevails upon the change of the other variables (S, TA,
422 DIC) in the tropical oceans and during the summer cyclonic season. However, a sharp
423 rise in pCO₂ has recently been reported after the passage of typhoon Choi-Wan in 2009
424 in the North West Pacific, which preceded the drop in temperature by about 6h [*Bond*
425 *et al.*, 2011]. Such short-term sequence could not be examined with the daily resolution
426 of our model outputs and deserves further investigation.

5.3. Caveats

427 Our results rely on an number of assumptions that were made to build the model.
428 Decreasing atmospheric pCO₂ during the passage of TCs, associated with the decrease
429 atmospheric pressure, have been reported [*Bates et al.*, 1998; *Huang and Imberger*, 2010],
430 with values up to 20 μatm (Sarma, unpublished data). In our model, the atmospheric
431 pCO₂ is increased from year to year but is not impacted by TCs. The model study of
432 *Huang and Imberger* [2010], which accounts for that effect, suggest that it is very short-
433 lived (<12h) and limited to the core of the TC (in a 50 km radius); we thus expect this
434 effect to be weak when averaged over the large oceanic area influenced by TCs.

435 Our results are also certainly dependent on the choice of the parameterization of the
436 gas transfer velocity at high wind speed, as suggested by the sensitivity analysis of *Perrie*
437 [2004]. A different choice might imply larger absolute values of the fluxes, and modulate
438 the strength of the compensations.

439 Another factor that was not accounted for in this study is the intense rain falls that
440 often come with TCs, and can dilute the salinity and DIC, with possible modifications
441 of the surface pCO₂. A more precise estimate of the TC induced F_{CO_2} would certainly
442 require to examine this aspect.

6. Conclusion

443 In this study, we used a state-of-the-art global ocean biogeochemical model driven by TC
444 wind forcing derived from a historical TC database. This allows us to examine the ocean
445 response along 1,663 TC tracks over the 1993-2007 period. The resulting modeled SST
446 response to TCs compares very well with satellite estimates during the same period. The
447 model also accurately reproduces the sharp pCO₂ drawdown recorded after the passage
448 of Hurricane Felix in 1995 in the NW Atlantic.

449 Previous case studies have illustrated the strong influence of TCs on ocean-atmosphere
450 CO₂ fluxes by increasing the gas exchange coefficient and decreasing the SST and oceanic
451 pCO₂. Moreover, it was generally assumed that the ocean is oversaturated in CO₂ under
452 TCs, because TCs blow essentially in the tropics during the summer season. Thus, based
453 on a these few observations, it has been suggested that TCs significantly increase the
454 CO₂ efflux from the ocean to the atmosphere. However, limited availability of pCO₂

455 observations under TCs harsh conditions has so far restricted global quantification of the
456 TC-induced F_{CO_2} to hazardous extrapolations.

457 We found a similar proportion of TCs over undersaturated regions ($\sim 20\%$ of TC loca-
458 tions are over regions where $DpCO_2 < -10\mu atm$) and oversaturated regions ($\sim 30\%$ for
459 $DpCO_2 > 10\mu atm$), with a large proportion ($\sim 50\%$) of TCs over regions where the ocean
460 and atmosphere are in near equilibrium. This estimation, based on our model outputs, is
461 consistent with a similar estimation from observed climatological pCO_2 variations. The
462 consequence is that TCs can generate instantaneous CO_2 fluxes directed from the ocean
463 to the atmosphere (efflux) or vice-versa (influx), depending on the oceanic condition at
464 the time of the TC passage; this instantaneous flux is very weak in $\sim 50\%$ of the cases.

465 Moreover, we identify two competing effects of TCs on F_{CO_2} that are not synchronous.
466 During the storm and depending on the sign of the difference of pCO_2 between the ocean
467 and atmosphere, TCs are responsible for large efflux or influx anomalies due to the strong
468 winds. During several weeks after the storm, oceanic pCO_2 is reduced in response to
469 vertical mixing, which systematically causes an influx anomaly. Generally, the storm
470 wind-effect and post-storm mixing effect have the same order of magnitude. This implies
471 that, contrary to previous estimates, TCs weakly impacts the CO_2 efflux because the
472 two effects oppose with each other when they blow over supersaturated areas (typically
473 in the North Atlantic, North-East Pacific, Arabian Sea). In contrast, TCs increase the
474 CO_2 influx because the two effects add up under undersaturated conditions (e.g. in the
475 Westernmost North Pacific, Bay of Bengal, South Indian and Pacific Ocean). In total, we
476 find that TCs account for $\sim 2\%$ of the F_{CO_2} during the cyclonic season over the tropical
477 ocean ($40^\circ N-40^\circ S$). This is an order of magnitude less than the lowest previous estimates.

478 Moreover, we find that regionally, TC account for 0 to 10% of the year-to-year variations
479 of the F_{CO_2} .

480 **Acknowledgments.**

481 This study was supported by IRD, CNRS, INSU (LEFE project CYCLOCEAN AO2010-
482 538863) and CNES (project CPUMP). Model development was supported by the NEMO
483 system team. The study was initiated during M.L., M.L. and E.M.V. stay at the NIO.

References

- 484 Aumont, O., and L. Bopp (2006), Globalizing results from ocean in situ iron fertilization
485 studies, *Global Biogeochem. Cycles*, *20*(2), 10.1029.
- 486 Babin, S., J. Carton, T. Dickey, and J. Wiggert (2004), Satellite evidence of hurricane-
487 induced phytoplankton blooms in an oceanic desert, *J. geophys. Res.*, *109*, C03,043.
- 488 Bates, N., A. Knap, and A. Michaels (1998), Contribution of hurricanes to local and global
489 estimates of air-sea exchange of co₂, *Nature*, *395*(6697), 58–61.
- 490 Bates, N. R. (2007), Interannual variability of the oceanic co₂ sink in the subtropical gyre
491 of the north atlantic ocean over the last 2 decades, *J. Geophys. Res.*, *112*(C9), C09,013.
- 492 Bond, N., M. Cronin, C. Sabine, Y. Kawai, H. Ichikawa, P. Freitag, and K. Ronnholm
493 (2011), Upper ocean response to typhoon choi-wan as measured by the kuroshio exten-
494 sion observatory mooring, *J. Geophys. Res.*, *116*.
- 495 Chiang, T.-L., C.-R. Wu, and L.-Y. Oey (2011), Typhoon kai-tak: An ocean’s perfect
496 storm, *Journal of Physical Oceanography*, *41*(1), 221–233, doi:10.1175/2010JPO4518.1.
- 497 Cione, J., and E. Uhlhorn (2003), Sea surface temperature variability in hurricanes: Im-
498 plications with respect to intensity change, *Monthly Weather Review*, *131*, 1783–1796.

- 499 Cravatte, S., G. Madec, T. Izumo, C. Menkes, and A. Bozec (2007), Progress in the
500 3-d circulation of the eastern equatorial pacific in a climate ocean model, *OCEAN*
501 *MODELLING*, *17*(1), 28–48, doi:10.1016/i.ocemod.2006.11.003.
- 502 D’Asaro, E. (2003), The ocean boundary layer below hurricane dennis, *Journal of physical*
503 *oceanography*, *33*(3), 561–579.
- 504 D’Asaro, E., and C. McNeil (2007), Air-sea gas exchange at extreme wind speeds measured
505 by autonomous oceanographic floats, *Journal of Marine Systems*, *66*(1-4), 92–109.
- 506 Donelan, M. A. (2004), On the limiting aerodynamic roughness of the ocean in very strong
507 winds, *Geophys. Res. Lett.*, *31*(18), L18,306, doi:10.1029/2004GL019460.
- 508 Gent, P. R., and J. C. McWilliams (1990), Isopycnal mixing in ocean circulation models,
509 *J. Phys. Oceanogr.*, *20*, 150–155.
- 510 Gierach, M. M., and B. Subrahmanyam (2008), Biophysical responses of the upper ocean
511 to major gulf of mexico hurricanes in 2005, *J. Geophys. Res.*, *113*(C4), C04,029.
- 512 Griffies, S. M., et al. (2009), Coordinated ocean-ice reference experiments (cores), doi:
513 10.1016/j.ocemod.2008.08.007.
- 514 Hanshaw, M. N., M. S. Lozier, and J. B. Palter (2008), Integrated impact of tropical
515 cyclones on sea surface chlorophyll in the north atlantic, *Geophys. Res. Lett.*, *35*(1),
516 L01,601.
- 517 Huang, P., and J. Imberger (2010), Variation of pco₂ in ocean surface water in response
518 to the passage of a hurricane, *J. Geophys. Res.*, *115*(C10), C10,024.
- 519 Koch, J., G. A. Mckinley, V. Bennington, and D. Ullman (2009), Do hurricanes cause sig-
520 nificant interannual variability in the air-sea co₂ flux of the subtropical north atlantic?,
521 *Geophys. Res. Lett.*, *36*(7), L07,606, doi:10.1029/2009GL037553.

- 522 Large, W. G., and S. G. Yeager (2009), The global climatology of an interannually varying
523 air-sea flux data set, *Clim Dyn*, *33*(2-3), 341–364, doi:10.1007/s00382-008-0441-3.
- 524 Liss, P. S., and L. Merlivat (1986), Air-sea gas exchange rates: introduction and synthesis,
525 in *The role of sea-air exchange in geochemical cycling*, vol. 185, pp. 113–127, Norwell,
526 Mass.
- 527 Liu, X., M. Wang, and W. Shi (2009), A study of a hurricane katrina-induced phyto-
528 plankton bloom using satellite observations and model simulations, *J. Geophys. Res.*,
529 *114*(C3), C03,023, doi:10.1029/2008JC004934.
- 530 Lloyd, I. D., and G. A. Vecchi (2011), Observational evidence for oceanic controls on
531 hurricane intensity, *J. Climate*, *24*(4), 1138–1153, doi:10.1175/2010JCLI3763.1.
- 532 Madec, G. (2008), Nemo ocean engine, *Note du Pole de modelisation de l’Institut Pierre-*
533 *Simon Laplace*, *27*, 1–217, doi:ISSN No 1288-1619.
- 534 Mahadevan, A., A. Tagliabue, L. Bopp, A. Lenton, L. Memery, and M. Levy (2011),
535 Impact of episodic vertical fluxes on sea surface pco₂, *Philosophical Transactions of the*
536 *Royal Society A: Mathematical, Physical and Engineering Sciences*, *369*(1943), 2009–
537 2025, doi:10.1098/rsta.2010.0340.
- 538 McNeil, C., and E. D’Asaro (2007), Parameterization of air-sea gas fluxes at extreme wind
539 speeds, *Journal of Marine Systems*, *66*(1-4), 110–121.
- 540 Nemoto, K., T. Midorikawa, A. Wada, K. Ogawa, S. Takatani, H. Kimoto, M. Ishii,
541 and H. Inoue (2009), Continuous observations of atmospheric and oceanic co₂ using a
542 moored buoy in the east china sea: Variations during the passage of typhoons, *Deep*
543 *Sea Research Part II: Topical Studies in Oceanography*, *56*(8-10), 542–553.

- 544 Patra, P. K., M. D. Kumar, N. Mahowald, and V. V. S. S. Sarma (2007), Atmospheric de-
545 position and surface stratification as controls of contrasting chlorophyll abundance in the
546 north indian ocean, *J. Geophys. Res.*, *112*(C5), C05,029, doi:10.1029/2006JC003885.
- 547 Perrie, W. (2004), The role of midlatitude storms on air-sea exchange of co₂, *Geophys.*
548 *Res. Lett.*, *31*(9).
- 549 Price, J. (1981), Upper ocean response to a hurricane, *Journal of Physical Oceanography*,
550 *11*, 153–175.
- 551 Price, J. F., J. Morzel, and P. P. Niiler (2008), Warming of sst in the cool wake of a
552 moving hurricane, *J. Geophys. Res.*, *113*(C7).
- 553 Sarmiento, J., and N. Gruber (2006), *Ocean Biogeochemical Dynamics*, 564pp pp., Prince-
554 ton University Press.
- 555 Son, S., T. Platt, H. Bouman, D. Lee, and S. Sathyendranath (2006), Satellite observation
556 of chlorophyll and nutrients increase induced by typhoon megi in the japan/east sea,
557 *Geophys. Res. Lett.*, *33*(5), L05,607, doi:10.1029/2005GL025065.
- 558 Takahashi, T., J. Olafsson, J. Goddard, D. Chipman, and S. C. Sutherland (1993), Sea-
559 sonal variation of co₂ and nutrients in the high-latitude surface oceans: A comparative
560 study, *Global Biogeochemical Cycles*, *7*(4), 843–878.
- 561 Takahashi, T., et al. (2009), Climatological mean and decadal change in surface ocean
562 pco₂, and net sea-air co₂ flux over the global oceans, *Deep Sea Research Part II: Topical*
563 *Studies in Oceanography*, *56*(8-10), 554–577.
- 564 Vincent, E. M., M. Lengaigne, G. Madec, J. Vialard, S. Masson, N. Jourdain, G. Sam-
565 son, and C. E. Menkes (2011a), Oceanic control of air-sea interactions under tropical
566 cyclones, *GRL*, *submitted*, 1–14.

- 567 Vincent, E. M., M. Lengaigne, G. Madec, J. Vialard, N. Jourdain, G. Samson, C. E.
568 Menkes, and S. Julien (2011b), Global study of processes controlling the ocean surface
569 cooling in the wake of tropical cyclones, *MWR*, *in preparation*.
- 570 Walker, N., R. Leben, and S. Balasubramanian (2005), Hurricane-forced upwelling and
571 chlorophyll a enhancement within cold-core cyclones in the gulf of mexico, *Geophys.*
572 *Res. Lett.*, *32*, 1–5.
- 573 Wanninkhof, R. (1992), Relationship between wind speed and gas exchange over the
574 ocean, *Journal of Geophysical Research*, *97*(C5), 7373–7382.
- 575 Willoughby, H., and M. Rahn (2004), 10d. 5 the climatology of hurricane wind profiles.
- 576 Willoughby, H., R. Darling, and M. Rahn (2006), Parametric representation of the pri-
577 mary hurricane vortex. part ii: A new family of sectionally continuous profiles, *Monthly*
578 *Weather Review*, *134*(4), 1102–1120.

	Total flux	TC-flux	% TC/Total	STD (Total/TC)
North Atlantic	-65.7 (-2699)	-0.6	+1%	11.1/1.8
North East Pacific	-130.0 (-4988)	-3.0	+2.3%	24.3/2.9
North West Pacific	+15.5 (+384)	+5.2	+33.4 %	21.8/2.3
Bay of Bengal	-0.6 (-117)	+0.1	-13.6 %	4.3/0.3
Arabian Sea	-43.4 (-2727)	-0.1	+0.2 %	6.1/0.2
South Indian	+93.1 (+2838)	+2.7	+2.9 %	26.8/1.2
Australia	+ 18.1 (+2017)	+0.5	+2.5 %	5.0/0.4
South Pacific	+53.3 (+2492)	+1.7	+3.2%	18.2/ 1.0
Total	-305.0 (-1258)	+6.7	-2.2%	85.0/5.0

Table 1. Regional and global CO₂ fluxes and contribution of TCs. Mean and standard deviation of total and TC-induced carbon flux cumulated over the cyclonic season and over different oceanic basins (delimited in Fig. 11), in Tera gC/cyclonic season. The STD represents interannual variations. The Total flux is computed over the region 40S-40N for the cyclonic season (NDJFMA for Southern Hemisphere and MJJASO for Northern Hemisphere). Value in parenthesis in the first column are in mgC/m².

	TC-flux $\Delta p\text{CO}_2 > 0$	TC-flux $\Delta p\text{CO}_2 < 0$	Days $\Delta p\text{CO}_2 > 0$	Days $\Delta p\text{CO}_2 < 0$
North Atlantic	+1.0	-1.6	16	80
North East Pacific	+0.3	-3.3	14	93
North West Pacific	+5.2	0.0	168	119
Bay of Bengal	+0.1	0.0	15	8
Arabian Sea	0.0	-0.1	0	13
South Indian	+2.5	+0.2	77	66
Australia	+0.5	0	19	27
South Pacific	+1.5	+0.2	45	24
Total	11.3	-4.6	354	430

Table 2. Global and Regional CO₂ fluxes due TCs depending on oceanic state. Mean TC-induced carbon flux cumulated over the cyclonic season (NDJFMA for Southern Hemisphere and MJJASO for Northern Hemisphere) and over different oceanic basins (delimited in Fig. 11). For each region, we count the number of TCs occurrences (In days/cyclonic season) and associated carbon flux (in Tera gC/cyclonic season) over undersaturated (versus oversaturated) oceanic state.

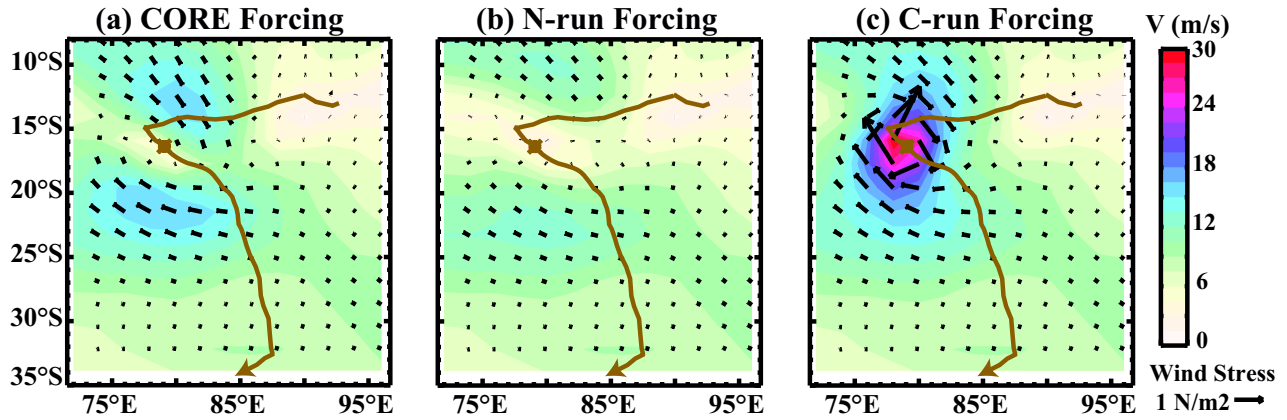


Figure 1. Illustration of forcing strategy to include TCs-related winds. Snapshot of the wind forcing on the 7th of April 1978 in the South-West Indian Ocean for: (a) COREforcing; (b) along-track filtered CORE forcing (N-run); and (c) along-track filtered CORE forcing superimposed with analytic TC vortices computed using IBTRACS TC location and maximum wind (C-run).

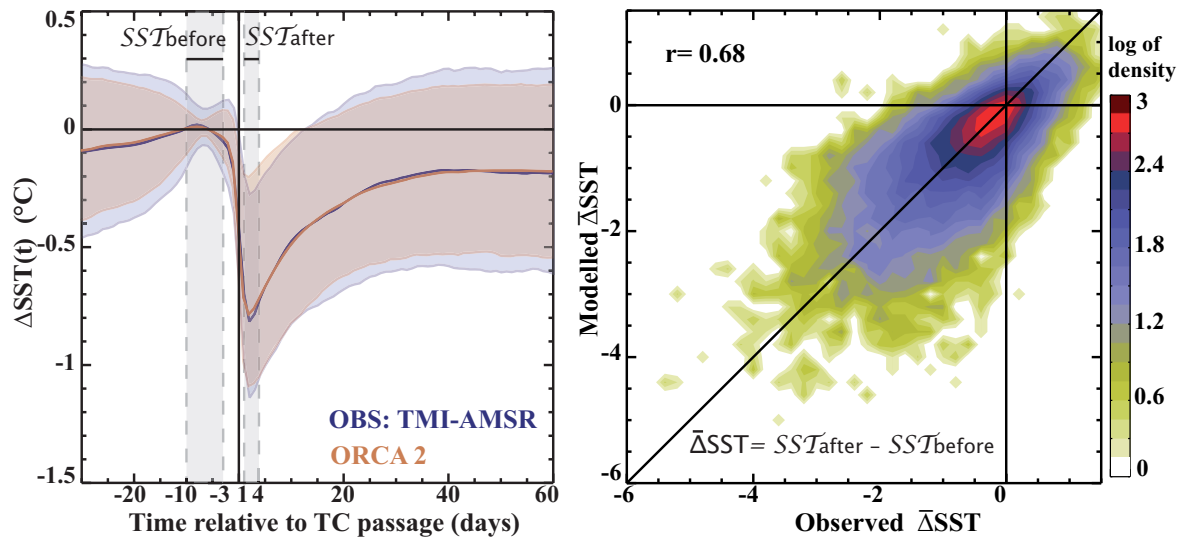


Figure 2. Evaluation of the timing and amplitude of surface temperature response to TCs (a) Temporal evolution of the mean TC-induced cooling along TC tracks for model and observations over the period 1998-2007. Shading indicates the spread around the mean value, calculated as $\pm 1/2$ quartile. (b) Probability Density function of simulated (C-run minus N-run) versus observed (TMI-AMSR) cold wake anomalies for the same period.

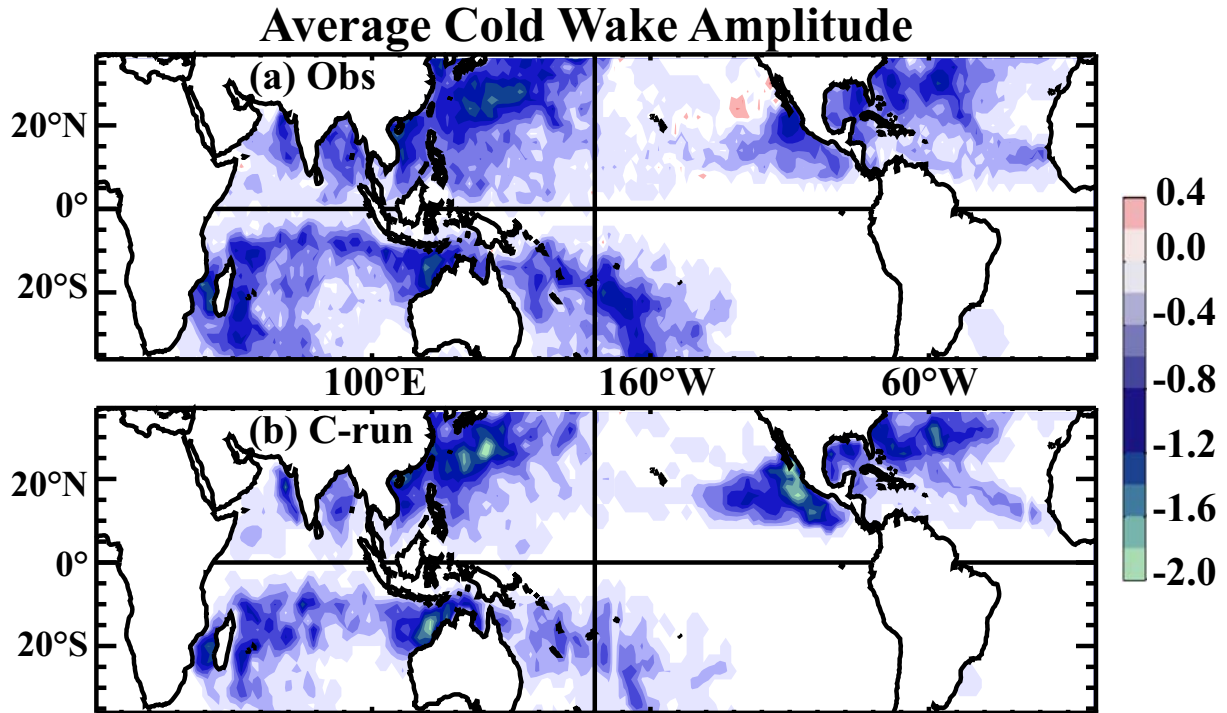


Figure 3. Evaluation of the spatial distribution of the surface temperature response to TCs. Spatial map of averaged cold wake anomaly amplitude (in °C) during the cyclonic season over the 1998-2007 period for (a) TMI-AMSR observations and (b) C-run.

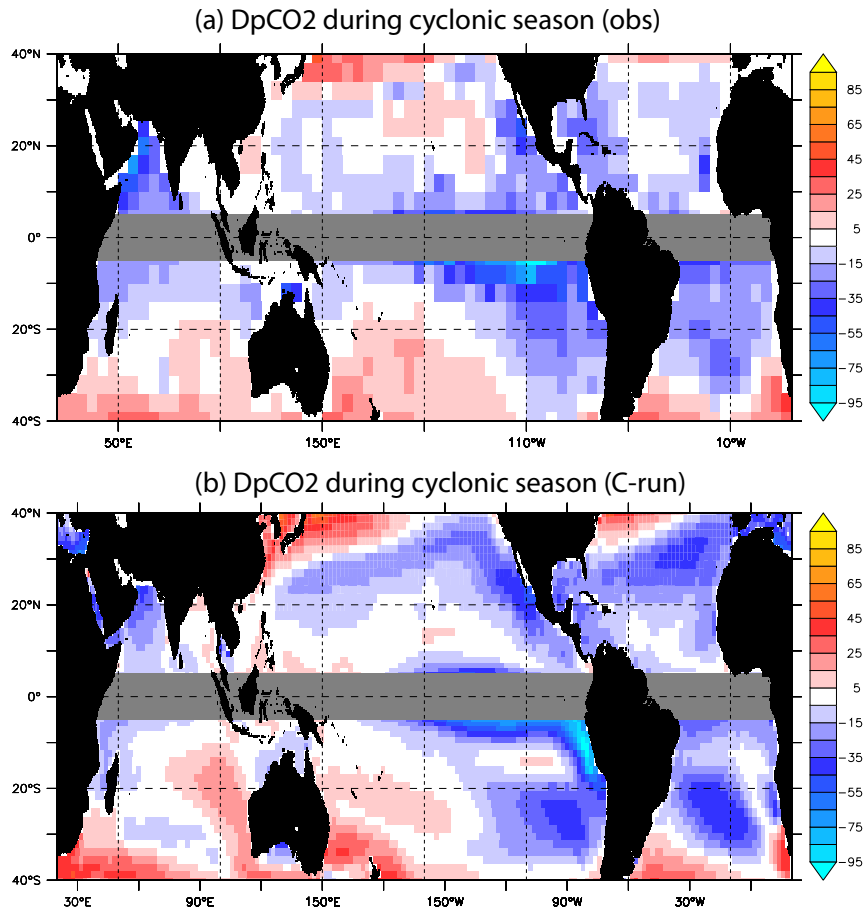


Figure 4. Evaluation of DpCO₂ during cyclonic season. DpCO₂ climatology (in μatm) during the cyclonic season (MJJASO in the northern hemisphere and NDJFMA in the southern hemisphere) from (a) Observed estimates [Takahashi *et al.*, 2009] and (b) the model (C run) over the 1993-2007 period. The grey band is to mark the time discontinuity between the two hemispheres.

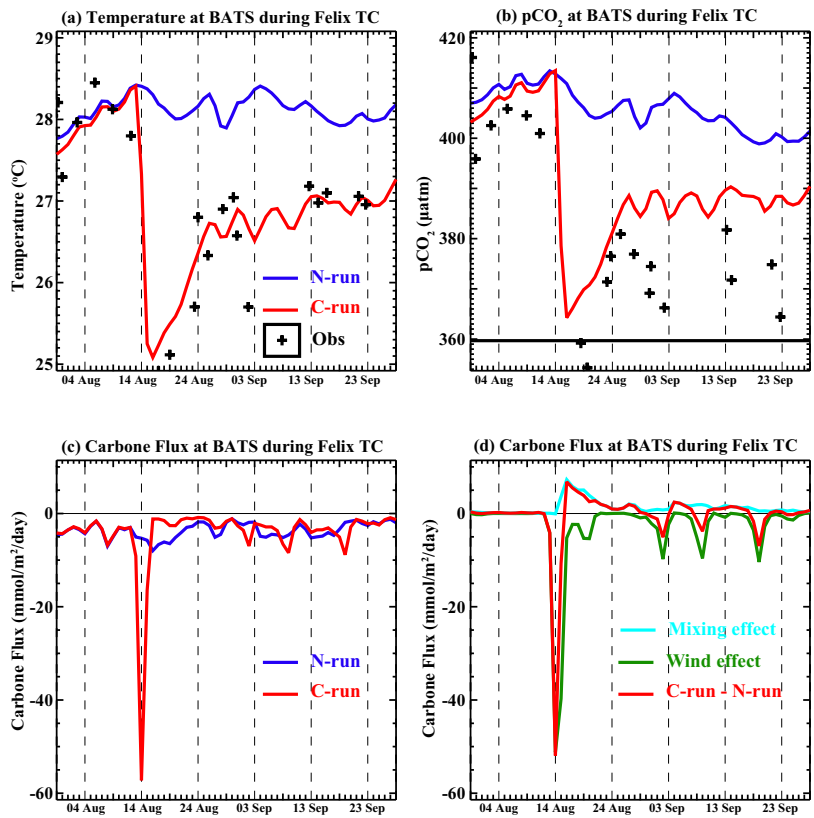


Figure 5. Hurricane Felix test case (BATS, August 1995). Temporal evolution of (a) SST and (b) oceanic pCO₂ (in μatm) in the C run (red), the N run (blue) and shipboard measurements from *Bates et al.* [1998] (dots) during the passage of Hurricane Felix in the Sargasso Sea near Bermuda in August 1995. (c) Temporal evolution of the air-sea CO₂ flux (negative when oriented from the ocean to the atmosphere in $\text{mmol}/\text{m}^2/\text{day}$) for the C run (red) and the N run (blue) (d) Temporal evolution of the flux difference between the C and N runs (red), flux anomaly related to the TC wind effect (green), flux anomaly related to the TC mixing effect (blue) (computed according to section 2.3).

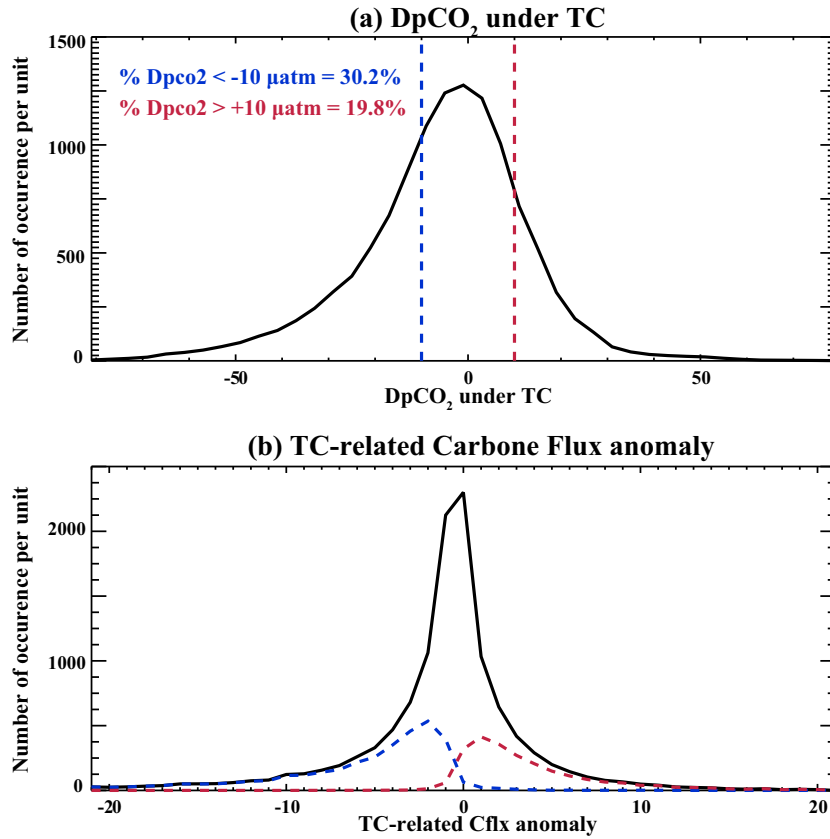


Figure 6. Distribution of $DpCO_2$ under TCs. Histograms of (a) $DpCO_2$ (in μatm) and (b) TC-related air-sea flux anomaly (in $\text{mmole}/\text{m}^2/\text{day}$) under TCs at time of maximum wind intensity for 46951 TC locations along 1663 TC tracks over the 1993-2007 period. Blue (red) curve on panel (b) correspond to the histogram of TC-related air-sea flux anomaly under cyclones where $DpCO_2 < 10 \mu\text{atm}$ ($DpCO_2 > 10 \mu\text{atm}$) corresponding to 30.2% (19.8%) of the cases.

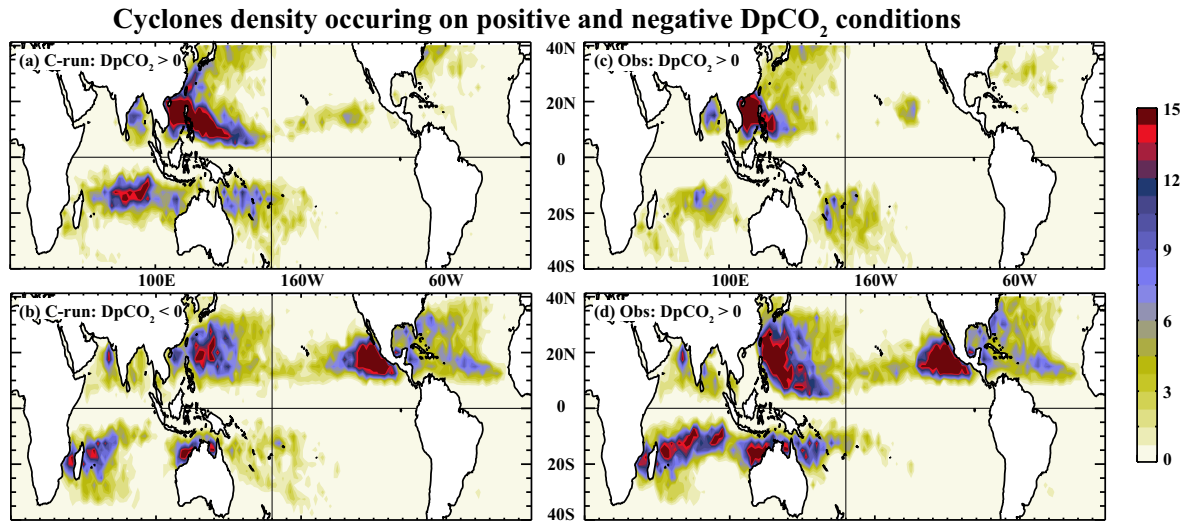


Figure 7. Locations where DpCO₂ is positive and negative under TCs. Density distribution (in cyclone-day/year) for TCs where (a) DpCO₂ > 0 and (b) DpCO₂ < 0 at $t=t_0$ in the C-run. Densities are computed over the 1993-2007 period. t_0 is the time of maximum wind intensity. (c) and (d) : same diagnostics applied to the DpCO₂ climatology of *Takahashi et al.* [2009] interpolated in time.

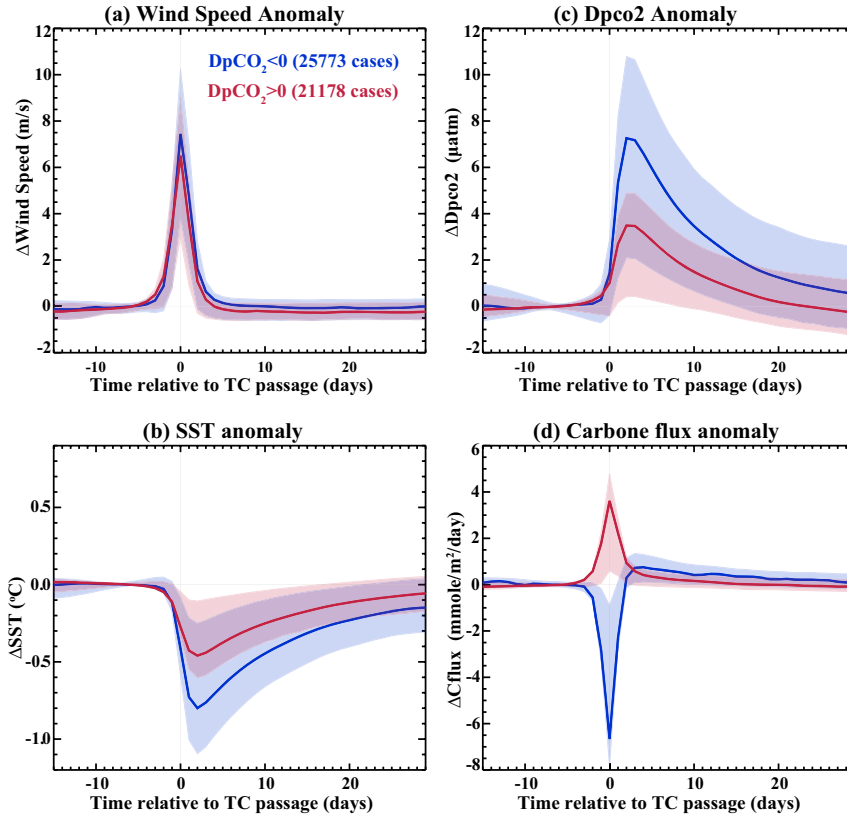


Figure 8. Composite time evolution of wind speed, SST, DpCO₂ and air-sea flux anomalies generated by the passage of TCs. Blue color: Mean composite of all cases (25773) where DpCO₂ < 0 at $t=t_0$, with t_0 the time of maximum wind intensity. Red color: Mean composite of all cases (21178) where DpCO₂ > 0 at $t=t_0$. Shading show the $\pm 1/2$ standard deviation around the mean composite value. Composites are computed over the 1993-2007 period. Anomalies are computed according to section 2.3.

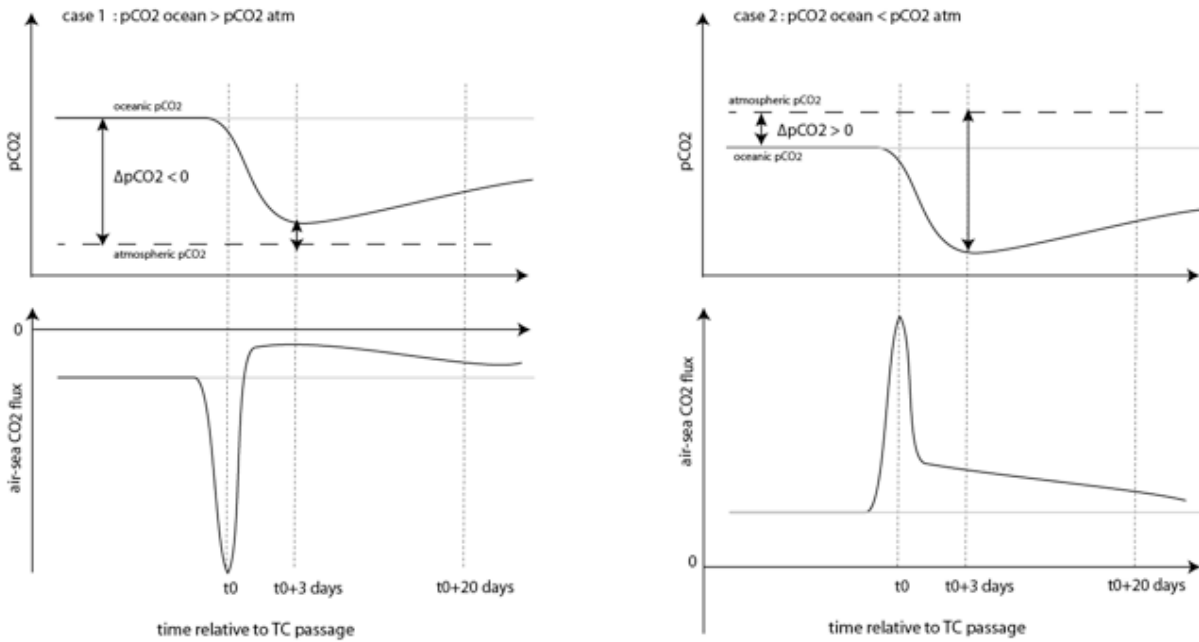


Figure 9. Schematic representation of the impact of TCs on pCO₂ and air sea flux.

Schematic time evolution of oceanic pCO₂ and air-sea CO₂ flux associated with the passage of a TC (black curves). For reference, the grey curves show the stationary situation in the absence of TC. Day t₀ is the time of maximum wind intensity during the passage of TC. The left column is the case where the oceanic pCO₂ is initially larger than the atmospheric pCO₂ and the air-sea flux is directed from the ocean to the atmosphere (case of BATS). The right column is when the atmospheric pCO₂ is initially larger than the oceanic pCO₂ and the air-sea flux is directed from the atmosphere to the ocean.

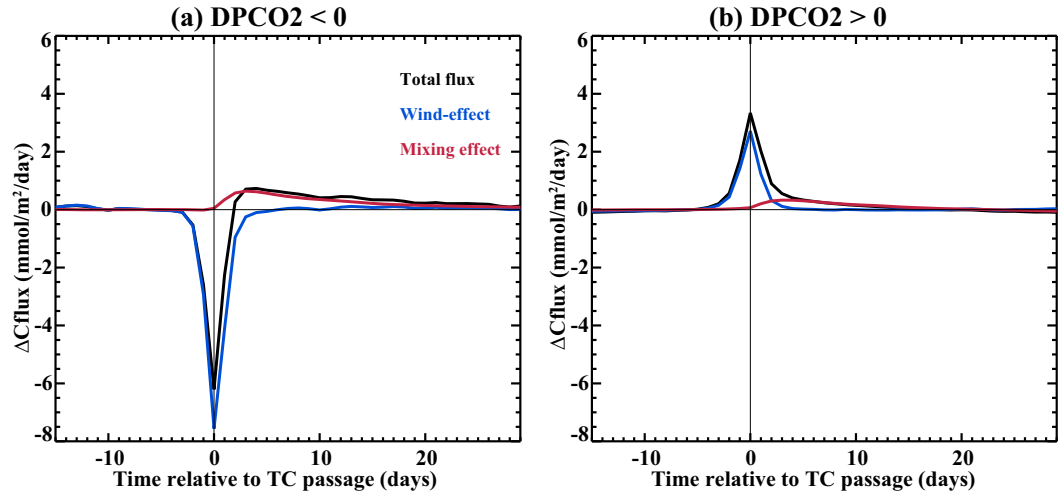


Figure 10. Composite time evolution of of TC-induced air-sea flux anomalies: **controlling mechanisms**. Mean of all cases where (a) $Dp\text{CO}_2 < 0$ at $t=t_0$ and (b) $Dp\text{CO}_2 > 0$ at $t=t_0$. Anomalies are computed over the 1993-2007 period. The black curve is the total TC-induced flux anomaly, the blue curve is the wind effect on the flux (section 2.3, equ. 2), the red curve is the mixing effect on the flux (section 2.3, equ. 3).

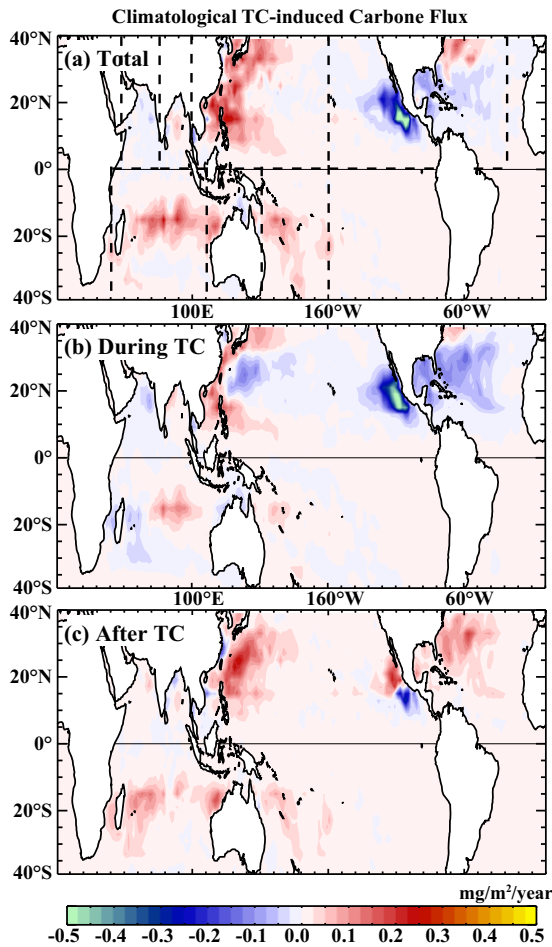


Figure 11. Climatological TC-induced air-sea flux. Climatological average of seasonally cumulated air-sea flux (in mmol/m²/season) induced by cyclones along their tracks in the C-run between (a) $t_0-1.5d$ and t_0+30d (b) $t_0-1.5d$ and $t_0+1.5d$ (c) $t_0+1.5d$ and t_0+30d . Dashed lines on panel (a) indicate the boundaries of the regions discussed in Tables 1 and 2.

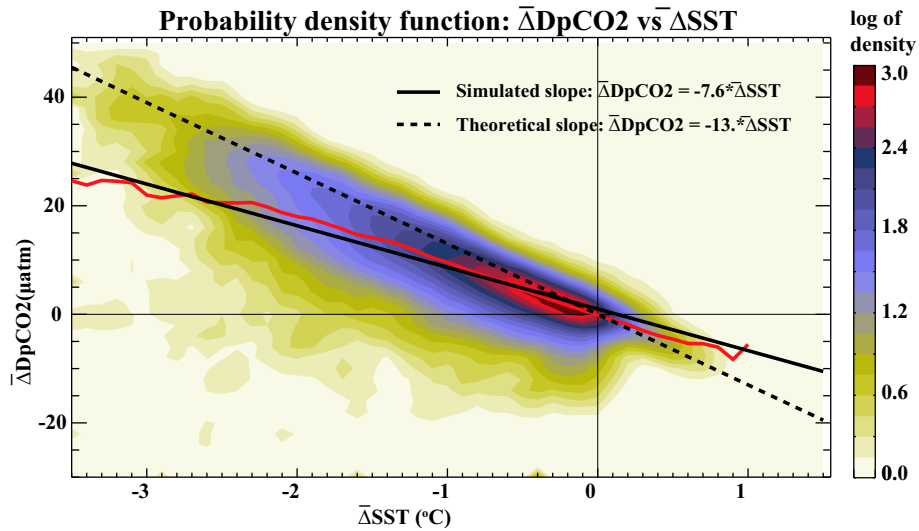


Figure 12. TC-induced DpCO₂ anomaly versus SST anomaly. Probability Density function of TC-induced DpCO₂ wake anomaly versus SST wake anomaly simulated in the model. Thick black line indicates the theoretical relationship of Gruber and Sarmiento, with a slope of -13. The blue line is the mean $\overline{\Delta SST}$ per bin of $\overline{\Delta DpCO_2}$. The black line is the linear fit to the blue line and as a slope of -7.6. Anomalies are computed over the 1993-2007 period along TC tracks for run C.